Journal of Materials Chemistry A

Acceleration of BODIPY dye-sensitized photocatalytic hydrogen production in aqueous ascorbic acid solutions using alkyl-chain formed second coordination sphere effects

Journal:	*Journal of Materials Chemistry A*
Manuscript ID	TA-ART-06-2023-003682.R2
Article Type:	Paper
Date Submitted by the Author:	28-Aug-2023
Complete List of Authors:	Shen, Xiao-Feng; Kyushu University, Department of Automotive Science Watanabe, Motonori; Kyushu University, International Institute for Carbon-Neutral Energy Research Song, Jun Tae; Kyushu University, Applied Chemistry Takagaki, Atsushi; Yokohama National University Graduate School of Engineering, Abe, Tatsuki; Center for Polymer Interface and Molecular Adhesion Science, Kyushu University, Tanaka, Keiji; Kyushu University, Applied Chemistry Ishihara, Tatsumi; Kyushu University, Department of Applied chemistry Faculty of Engineering

ARTICLE

Acceleration of BODIPY dye-sensitized photocatalytic hydrogen production in aqueous ascorbic acid solutions using alkyl-chain formed second coordination sphere effects

Received 00th January 20xx,
Accepted 00th January 20xx

DOI: 10.1039/x0xx00000x

Xiao-Feng Shen [a], Motonori Watanabe [a,b,c,d*], Jun Tae Song [b,d], Atsushi Takagaki [e], Tatsuki Abe [f], Keiji Tanaka [a,b,d,f], Tatsumi Ishihara [a,b,c,d]

BODIPY (boron−dipyrromethene) compounds are extensively utilized in various applications. Typically, their activity is modified by altering the functional groups at the α−, β−, and meso− positions of the substituents. However, no systematic information is provided on the effect of substituted F−positions and hydrophobicity on the activity of BODIPY sensitizers in photosensitizing chemistry. Dyes (**7a**-**7c**) with different alkyl chain lengths were synthesized and compared with unsubstituted **3** to discuss the effect of −F position substituents and hydrophobicity of BODIPY dyes on photocatalytic activity. Density functional theory (DFT) calculations showed that −F substitution induced an intramolecular charge transfer (ICT) effect, enhancing visible light absorption. Longer alkyl chains provide a favourable second coordination sphere reaction environment for hydrogen production. Experimentally, dye **7c** demonstrated the highest activity, with a hydrogen production rate of 496.5 $\mu mol \cdot gcat^{-1} \cdot h^{-1}$ which is 3 times higher than **3**, and 9.6 times higher turnover frequency (TOF) than **3**. An apparent quantum yield (AQY) at 650 nm showed 1.4%. This study highlights the importance of −F position substitution and optimizing hydrophobicity to enhance the photocatalytic activity of metal-free organic dyes through the creation of a new second coordination sphere.

1 Introduction

Dye−sensitized charge transfer mechanism in organic-inorganic hybrid system are widely used in solar cells,[1] artificial photosynthesis,[2] and photocatalytic water splitting for hydrogen production.[3] Among them, photocatalytic water splitting for hydrogen production is a sustainable and eco-friendly method for hydrogen production, which has received wide attention.[4,5] Titanium dioxide (TiO_2) is a semiconductor material that is widely used in dye−sensitized catalysts.[6,7] In dye-sensitized TiO_2 photocatalytic system, dye molecules adsorbed on the surface of TiO_2 can enhance the light absorption ability of TiO_2, thus improving the efficiency of photocatalytic decomposition of water splitting.[8] Photocatalytic hydrogen production is a complex reaction. Not only the catalyst properties can change the catalytic activity, but also the catalyst environment can greatly change the reaction rate.[9,10] By varying the hydrogen bonding, electrostatic interactions, and substrate/reactant channels, the environment of catalyst can be changed for the improvement of the activity and stability.[11] Recently, the second coordination sphere effects, which refers to the external factors and environment that influence the properties and reactivity of a molecule or ion indirectly, have been widely studied and discussed in the photocatalytic reaction including CO_2 photoreduction.[12,13] New reaction environment formed organic component on the surface of inorganic catalysts can improve catalytic activity. For example, Wu et al. used supramolecular (polyethyleneimine) interaction to construct the secondary coordination sphere on CdSe quantum dots to let hole removal much faster, thus leading to higher stability and photocatalytic activity for H_2 evolution.[14] Huang et al. reported that poly dimethyl siloxane coated catalysts prevent Pd aggregation and further reduce surface wettability and improves contact for organic reactant.[15] Li et al. reported hydrophobic treatment of the MOF pore significantly enhancement activity and selectivity to organic oil.[16] These previous studies indicated that hydrophobic treatments are known to be an important factor to change the reaction environment of catalyst. Recently, Sinha et al. proposed hydrophobic substrates can form hydrophobic interlayers or hydrophobic shells on the catalyst and make a new secondly/outer coordination sphere in molecular catalyst.[17] These previous studies indicate that if coordination spheres can be formed by designing the structure of the dye molecule as a hydrophobic moiety at the organic/inorganic hybrid catalyst interface, it is possible to increase the catalytic activity in the dye-sensitized catalyst system. BODIPY is a class of organic compounds that are widely used in various fields such as fluorescent probes,[18] and cancer phototherapy[19] due to their unique

[a] *Department of Automotive Science, Graduate School of Integrated Frontier Sciences, Kyushu University, 744 Motooka, Nishi-ku, Fukuoka, 819-0395 (Japan).*
[b] *International Institute for Carbon-Neutral Energy Research (WPI-I2CNER), Kyushu University, 744 Motooka, Nishi-ku, Fukuoka, 819-0395 (Japan).*
[c] *Center for Energy Systems Design (CESD), Kyushu University, 744 Motooka, Nishi-ku, Fukuoka, 819-0395 (Japan).*
[d] *Department of Applied Chemistry, Faculty of Engineering, Kyushu University, 744 Motooka, Nishi-ku, Fukuoka, 819-0395 (Japan).*
[e] *Division of Materials and Chemical Engineering, Faculty of Engineering, Yokohama National University, 79-5 Tokiwadai, Hodogaya-ku, Yokohama, 240-8501 (Japan)*
[f] *Center for Polymer Interface and Molecular Adhesion Science, Kyushu University, 744 Motooka, Nishi-ku, Fukuoka, 819-0395 (Japan).*

† Electronic Supplementary Information (ESI) available: [Dye synthesis, UV, FL, DFT, photocatalytic activity, time-resolved absorption spectra, ^1H NMR, ^{13}C NMR and ^{19}F NMR spectra]. See DOI: 10.1039/x0xx00000x

photophysical properties. BODIPY dyes have also been studied as active materials in dye-sensitized catalysts[20] due to their strong light absorption and high molar extinction coefficient.[21] Most of the donor (D)−π−acceptor (A) type BODIPY dyes are generally discussed by modulating and changing the functional groups at the α− , β− and meso− positions of the substituents to affect the activity.[22,23] On the other hand, functionalization of the boron atom of BODIPY by fluorine substitution of the boron-fluorine bonding moiety can improve the stability of the dye by altering its electronic properties.[24] Few articles have investigated the effect of substituted F positions on the changes.[25,26] There are no studies discussing the physical properties and photocatalytic activity effects of substitution of fluorine on boron-fluorine moieties for dye-sensitized catalyst systems. To understand the chemical and physical properties of the hydrophobic groups that affect the photocatalytic efficiency, in this report, we systematically designed and prepared a series of three hydrophobic materials with the different alkyl chains (**7a**–**7c**) and compared them with the less-hydrophobic compound (**3**), and reported the second coordination sphere effects for boosting of the photocatalytic hydrogen production property.

2 Experimental

2.1 General information

^{1}H,^{13}C, and ^{19}F NMR spectra were recorded on Bruker AV400 (400 MHz) spectrometers. UV-vis absorption and diffuse reflectance spectra were recorded on a Shimadzu UV-3600 spectrophotometer. The diffuse reflectance spectra (DRS) of the catalyst were measured using 2 wt% catalyst–$BaSO_4$ pellets. The photoluminescence spectra were measured by fluorescence spectrophotometer (F-7000, HITACHI). Cyclic voltammetry (CV) was obtained using an electrochemical analyzer (BAS ALS-1200B).

2.2 Density functional theory (DFT) calculations

All calculations were performed using the Gaussian 16, Revision A.03 suite of program. Geometry optimizations and time-dependent density-functional theory (TD-DFT) calculations for **3** and **7a-c** were performed by using Becke's three-parameter hybrid functional (B3) with the correlation functional of Lee, Yang, and Parr (LYP) and the Pople style basis set 6-31G(d). Gaussview 6.0 was utilized to visualize the distribution of the highest occupied molecular orbital (HOMO) and lowest unoccupied molecular orbital (LUMO). The resulting absorption spectral values were processed and analyzed using Gauss Sum[27].

2.3 Photocurrent and impedance measurement

A conventional three-electrode configuration was used. The **dye**/TiO_2/ fluorine-doped tin oxide (FTO) electrode used as the working electrode, was made through four steps. First, the FTO glass was cleaned by ultrasonic cleaning in acetone and isopropyl alcohol, respectively, for 15 minutes each. Second, ozone cleaning was performed for 10 minutes. Next, the TiO_2/FTO electrode was fabricated using the Squeegee method and annealed at 500 °C for 5 hours in an air atmosphere. Finally, the TiO_2/FTO electrode was immersed in a **dye** THF solution for 24 hours and subsequently washed with a THF solution. The platinum wire as the counter electrode, and Ag/AgCl (in 3.0 M KCl) as the reference electrode was employed. All the measurements were performed in DI water solutions containing 0.1 M Na_2SO_4 and 0.57 M ascorbic acid as the supporting electrolyte (pH 4.0). The photocurrent properties were obtained under irradiation with a 300 W Xe lamp (Asahi Spectra, MAX-303) using a long-pass filter (Edmund optics, >420 nm filter). The photocurrent was measured using a BAS ALS1200B instrument.

2.4 Photocatalytic hydrogen production

The photocatalytic hydrogen production reaction was performed using a solar simulator (MAX-303, Asahi Spectra, Japan, 0.15 W cm^{-2}, >420 nm filter) a quartz-closed, reactor circulating system equipped with a thermal conductivity detector (Ar carrier, column: molecular sieve 4Å, Shimadzu, Japan, GC-8A), and 20 mg of catalyst powder were added into an ascorbic acid (0.57 M, 20 mL, pH 4.0) solution. The turnover number and frequencies were calculated using the following eq 1 and eq 2:

$$\mathrm{TON} = \frac{2 \times \text{number of evolved } H_2 \text{ molecules}}{\text{number of dye molecules adsorbed}} \quad \text{eq. 1}$$

$$\mathrm{TOF} = \frac{\mathrm{TON}}{\text{reaction time}} \quad \text{eq. 2}$$

Apparent quantum yields (AQYs) were determined for **7c**/Pt-TiO_2 at wavelengths of 600, and 650 nm. The experiments were performed over same with photocatalytic hydrogen production. The light intensity was measured using an ADCMT 8230E optical power meter. The AQYs were calculated according to the following eq 3:

$$\mathrm{AQY}\ (\%) = \frac{n \times N_A \times h \times c}{I \times A \times \lambda \times T} \times 100 \quad \text{eq. 3}$$

where, n (mol) is the moles of photogenerated H_2, N_A (mol^{-1}) is the Avogadro constant, h (J s) is the Planck constant, c (m s^{-1}) is the speed of light, λ (m) is the wavelength, T (s) is the irradiation time, I (W m^{-2}) is the light intensity, and A (m^2) is the irradiated area.

2.5 Water contact angle measurement

Water contact angle measurement (DMo-601, KYOWA) provides hydrophilic characterizations of membranes. DI water was used as a probe liquid and when DI water droplet of 2 µL was put on the **dye**/TiO_2 film surface, the water contact angle was averaged at three points of each film.

2.6 Zeta potential

Zeta potentials were measured by Zeta-potential Analyzer (ELSZ-2000, OTSUKA Electronics). A 1 mg of catalyst powder was suspended to 5 mL of water (pH=4.0) for 30 min by ultrasonication. Then, the reaction solution was added to the device and electrophoretic light scattering (ELS) was used to measure the Zeta potentials. The concentration (mol/L) of the adsorbed ascorbic acid ions (C_s) were calculated according to the following eq 4:

$$C_s = C_B\, exp(e \times \Psi / \kappa T) \quad \text{eq.4}$$

where, C_B (mol/L) is the concentration of ascorbic acid, e (C) is the

elementary charge, κ (J/K) is the Boltzmann constant, T (K) is the absolute temperature, and Ψ (V) is the zeta potential (ζ).[14]

2.7 Time-resolved absorption measurements

Femtosecond time-resolved absorption data were collected using a pump–probe time-resolved absorption spectroscopy system (Ultrafast Systems, Helios). The pump light (400 nm) with a pulse width of 100 fs at a repetition rate of 1 kHz was generated by Ti-sapphire laser system (Spectra-Physics, Solstice). Detection was performed in the UV–vis range (450–750 nm) using a linear CCD array (Ultrafast Systems, CAM-VIS-2). The data were fitted with the following double exponential decay function eq 5:

$$= A_0 + A_1 \exp\left[-\frac{t}{\tau_1}\right] + A_2 \exp\left[-\frac{t}{\tau_2}\right] \qquad \text{eq. 5}$$

where, A_0, A_1, A_2 are constant values, t is experimental data, τ_1,τ_2 are time decay constants.

3 Results and discussion

3.1 Synthesis of dye sensitizer

Synthesis of dye sensitizers are showed in Scheme 1. Pyridine−bodipy **3** was synthesized by reaction with 2,4−dimethyl−1H−pyrrole **1** and 4−pyridinecarbaldehyde **2** in the catalytic amounts of trifluoroacetic acid (TFA), followed by oxidized with 2,3−dichloro−5,6−dicyano−p−benzoquinone (DDQ), and complexed with boron trifluoride−ethyl ether complex ($BF_3{\cdot}Et_2O$) to obtain a yield of 20%. And precursors **6b**-**6c** were obtained from hydroquinone **4** with 1−bromopentane **5b** and 1−bromododecane **5c** catalysed by potassium carbonate to obtain a yield of 28−48%. Dye sensitizers **7a**−**7c** were synthesized by −BODIPY **3** and **6a**−**6c** with anhydrous aluminium chloride as 20−30%.

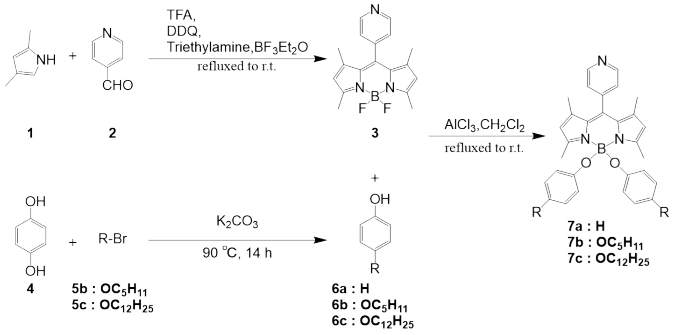

Scheme 1. Synthetic route of BODIPY-sensitizers.

3.2 Optical properties

Fig. 1a shows UV−vis absorption spectra of **7a-7c** in THF solution, which exhibits a sharp absorption peak with a high molar extinction coefficient. Precursor **3** shows the absorption maximum at 503 nm and the molar extinction coefficient (ε) of 52000. After changing −F to alkoxy phenyl group, the absorption maximum shifted from 503 nm to 506 nm and the molar extinction coefficient became 76000 for **7a**, 71000 for **7b** and 69000 for **7c**. However, as the alkyl chains become longer, no shift in the absorption maximum can be observed, only a decrease in the molar extinction coefficient. Furthermore, compared with **3**,**7a**-**7c** found a weak-broad new absorption around 560-750 nm. To gain further insight into this area, the UV-vis spectra of a highly concentrated (2×10^{-4} M) dye were measured (Fig. S1). Although the peak in the 420-550 nm range exhibits absorption saturation in the experiment condition, it is significant to emphasize that a distinct peak at 598 nm with a molar extinction coefficient (ε) of 82-105 can be observed. The diffuse reflectance absorption spectra displayed in Fig. 1b showed the appearance of an absorption peak at 400-570 nm after **3** loaded, while for after **7a**-**7c** loaded on Pt-TiO_2 the absorption between 400−750 nm can be observed, which indicates that all 4 kinds of **3** and **7a**-**7c**/Pt-TiO_2 can absorb the visible light, with a same absorption maximum at 519 nm. Compared with the spectrum of **3** and **7a**-**7c** in THF solution, the absorption maximum was red-shifted in **3** and **7a**-**7c**/Pt-TiO_2, which is indicative of a J−type aggregation between the dye molecules.[28] A new band at 500-750 nm present in **7a–7c** was assigned to the intramolecular charge transfer (ICT) band occurring between the BODIPY core and the alkoxy phenyl group (discussed later in the DFT section). The absorption intensity of ICT band increased in **7a-7c**/Pt-TiO_2 compared to THF solution. Tang et al. reported that in a system in which a donor-acceptor molecule was introduced into BODIPY, the intramolecular rotation of aggregates affected the interaction of intramolecular orbitals and controlled the photo-induced property such emission intensity.[29] In the case of **7a-7c**/Pt-TiO_2, this is probably because aggregation inhibits the free rotation of the alkoxy phenyl groups and increases the transition probability. The dye loading amount was estimated to be 17.8 μmol/g for **3**, 38.4 μmol/g for **7a**, 10.7 μmol/g for **7b**, 5.5 μmol/g for **7c**. Thus, it can be found that as the alkyl chain increases, the dye load amount becomes less. Since the increase of alkyl chains, which makes the chance of dye molecules colliding with each other, which leads to a lower loading amount. Meantime, a peak at 519 nm can be observed in the fluorescence spectra, with no variation in emission maximum between each dye, only the intensity becomes lower, during the alkyl chains become longer. The stokes shift of each dye are 12−15 nm, $E_{0\text{-}0}$ transition energy band of dye is 2.44 eV of **3**, 2.43 eV of **7a**−**7c**, according to the intersection of absorption and photoluminescence spectra (Fig. S2). These results suggest that O-phenyl substitution at the fluorine site does not significantly change the energy gap.

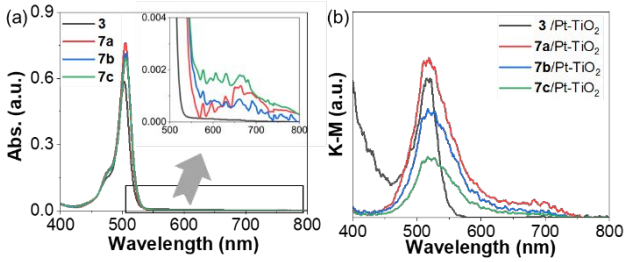

Fig. 1 (a) UV–vis absorption spectra of dye in THF solution. (b) Diffuse reflectance absorption spectra of **dye**/Pt-TiO_2.

3.3 Electrochemical properties

To examine the HOMO and the LUMO, cyclic voltammetry experiments were performed in 0.1 M nBu_4NPF_6 in THF solution (Fig. 2a). The results showed an oxidation peak at +1.37 V (vs. NHE), a reduction peak at −0.99 V (vs. NHE) of precursor **3**, the HOMO level shows +1.35 V (vs. NHE), the LUMO level shows −1.08 V (vs. NHE) of **7a**, while +1.30 V (vs. NHE), −1.13 V (vs. NHE) of **7b**, and +1.29 V (vs.

NHE), −1.14 V (vs. NHE) of **7c**. No change between **7b** and **7c**, even though the alkyl chains became longer. The HOMO−LUMO gap shows 2.43 eV of **7a**-**7c**, which was same to the energy gap calculated from the UV−vis absorption spectra (2.43 V). Fig. 2b showed energy diagram of dye, for TiO_2, the conduction band (CB) is −0.45 V (vs. NHE), which is more negative than the LUMO level of the **3** and **7a**-**7c**, indicating that electrons can be transferred from the **3** and **7a**-**7c** to TiO_2.[30]

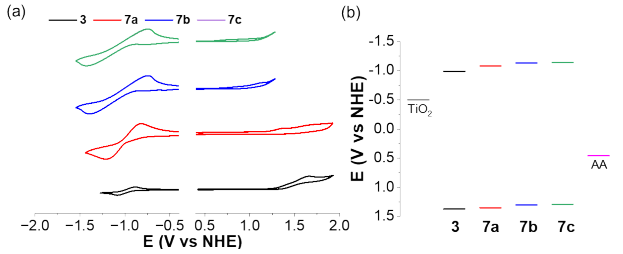

Fig. 2 (a) CV plots of **3** and **7a**-**7c** in THF solution. (b) energy diagram of TiO_2, **3,** and **7a**-**7c** (AA, ascorbic acid as the sacrificial agent).

3.4 DFT calculation

Theoretical calculations are widely applied to the analysis of the properties of organic molecules.[31] Here, the optimized structure of dye was determined via DFT calculations. Fig. S3 shows the absorption spectra under theoretical calculations. As shown in Fig. S3b, for **3**, the peak near 409 nm belongs to HOMO to LUMO transition, and since both HOMO and LUMO of **3** are only delocalized over BODIPY structure which can prove this peak belongs to π–π* transition, and not occupied on fluorine atom, which means no intramolecular charge transfer (ICT) between BODIPY moiety and fluorine atom occurred. The absorption maximum of the **7a**-**7c** is 412 nm in the theoretical calculation, which is attributed to HOMO (BODIPY core) → LUMO (BODIPY core) for **7a**, and HOMO-2 (BODIPY core) → LUMO (BODIPY core) for **7b** and **7c**. Combined with Fig. 3, it can be concluded that this peak also belongs to π- π* transfer. On the other hand, as compared to **3**, a new absorption in the long wavelength range is shown in **7a**-**7c**. The weak absorption peaks at 607 nm are identified as HOMO-1 (BODIPY core and a part of phenyl group) → LUMO (BODIPY core) for **7a**, and HOMO (alkoxy-phenyl group) → LUMO (BODIPY core) for **7b** and **7c**. It can be concluded that this peak belongs to ICT. As the alkyl chains becomes longer, the HOMO distribution gradually shifts from the BODIPY skeleton to the phenyl moiety. Moreover, there is no charge distribution of HOMO and LUMO on the alkyl chain. From the DFT calculation and UV−vis absorption spectra, the absorption peak **7a**-**7c** at 503 nm belongs to π- π* transition, and peak between 560 and 750 nm occurred due to ICT.

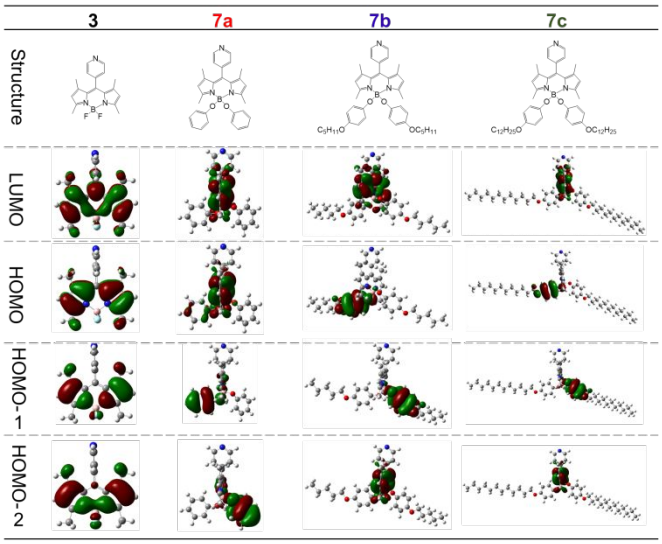

Fig. 3 Structure, HOMO and LUMO orbitals of **3** and **7a**-**7c** (B3LYP/6-31G(d))

3.5 Water contact angle

To reveal the effect of alkyl chains on interface between dyes and sacrificial agents, the surface information of the photocatalyst was investigated by the water contact angle (Fig. 4). The water contact angle of the **3**/TiO_2 electrode was 25.3 degrees. With the introduction of alkyl chains, the water contact angle gradually increased from 39.1° (**7a**) to 46.4° (**7b**) and then to 57.2° (**7c**). These results were demonstrated that the hydrophobicity of the dye becomes stronger with the increase of the alkyl chains.

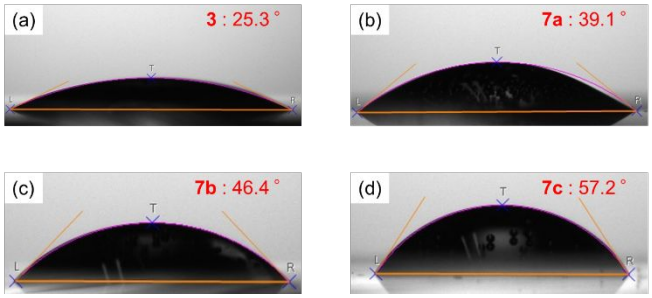

Fig. 4 Water contact angle of **Dye** /TiO_2: (a) **3**; (b) **7a**; (c) **7b**; (d) **7c**.

3.6 Photocatalytic activity

To investigate the photoactivity of dye sensitizers, photocatalytic reactions were conducted using **3** and **7a**-**7c**/Pt−TiO_2 as a photocatalyst and ascorbic acid (pH 4.0) as a sacrificial agent under irradiation with a Xe lamp (>420 nm filter, Fig. 5a). **7c** showed the best hydrogen production activity within 4 kinds of dye as 496.5 $\mu mol \cdot g_{cat}^{-1} \cdot h^{-1}$. **7b** showed second higher activity as 394.5 $\mu mol \cdot g_{cat}^{-1} \cdot h^{-1}$. Then, **7a** showed hydrogen activity as 325.5 $\mu mol \cdot g_{cat}^{-1} \cdot h^{-1}$. In contrast to those precursors **3**, only showed 166.1 $\mu mol \cdot g_{cat}^{-1} \cdot h^{-1}$ for hydrogen activity. Turnover number can remove the effect of dye loading amount; therefore, it is one of the important criteria to evaluate the catalyst performance (Fig. S4). Turnover frequencies (TOFs) were also calculated for the four dye sensitizers over a 5-hour period. The TOF values of dye sensitizer of the order was allowing as **7c** (180.5 h^{-1}) > **7b** (73.8 h^{-1}) >**7a** (19.0 h^{-1}) ≈ **3** (18.6 h^{-1}). The results of **7c** showed that 3 times higher hydrogen

production rate than **3**, and 9.6 times higher TOF than **3**. Same loading amount (5.0 μmol/g) of **3** and **7a**-**7c** /Pt-TiO_2 were also measured (Fig. S5). The catalytic activity of dye sensitizer of order was also allowing as **7c** > **7b** > **7a** > **3**. As the alkyl chain increases, the photocatalytic activity of dye sensitizers becomes higher. Furthermore, hydrogen cannot be produced in the presence of ascorbic acid only (Fig. S6). As such, the best hydrogen production activity was shown by **7c**. Apparent quantum efficiency (AQY) is a key parameter for determining the efficiency of photocatalytic processes.[32] The AQY values of **7c**/Pt−TiO_2 were determined to be 2.2%, and 1.4% with band path filters of 600, and 650 nm, respectively.

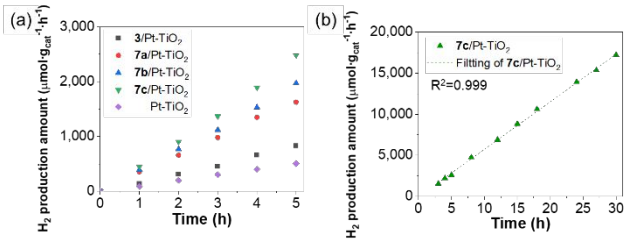

Fig. 5 (a) Photocatalytic hydrogen production results of **3** and **7a**-**7c**/Pt-TiO_2. (b) Long-time reaction test of **7c** /Pt-TiO_2.Conditions: Xe lamp (0.15 W cm^{-2}, >420 nm), 0.57 M ascorbic acid aq. (pH 4.0).

To check the stability of **7c**, the photocatalytic activity experiment was performed over 30 h as shown in Fig. 5b and six times over 4 h as shown in Fig. S7. Hydrogen production amount showed a linear relationship. Also, UV−Vis, and ^{1}H NMR were used to confirm the state of the **7c**/Pt−TiO_2 after the reaction. The powder was separated from the reaction solution by centrifugation, and the organic components of the reaction solution was extracted with $CDCl_3$. As shown in Fig. S8, no peak represented **7c** was observed in the after-reaction solution. The ^{1}H NMR result also demonstrated that no dye was detached from TiO_2 (Fig. S9). Compared with other reported dye-sensitized photocatalyst performances are summarized in Table S1, Other BODIPY sensitizer system or carbon nanotube-fullerene composite photocatalysts showed higher AQY (1.4-3.6%) at 650 nm, but activity decreased by 8-66% within 30 h. The benzothiadiazole polymer, porphyrin, and phthalocyanine sensitized systems showed lower AQY (0.4-1.1%) than **7c**/Pt-TiO_2 and decreased activity (~33%). We previously reported a squarinic dye sensitizer system with a very high AQY (12.5%@650 nm), but this system showed 10% deactivation in 30 hours.[8] The BODIPY system in this report not only has an activity comparable to that of AQY (1.4%@650 nm) in other reports but is also a stable photocatalytic hydrogen production system that does not undergo any decomposition even after 30 hours.

3.7 Zeta potential experiment

To examine the electron donating/accepting ability between the ascorbic acid/dye sensitizer, zeta potential experiments were measured. The zeta potential of Pt-TiO_2 (pH=4.0 in water) showed a negative charge of -33.8 mV. Ascorbic acid takes on a neutrally charged structure in acidic conditions (pH = 4.0), and as the pH moves to basic, it releases protons and changes to an anionic species of ascorbate form.[33] The zeta potential of ascorbic acid aqueous solution (pH=4.0), which is not ascorbate structure, showed positive value of +16.92 mV. The zeta potentials of **dye**/Pt-TiO_2 in water at pH 4.0 were all negative values following as **3** (-0.3 mV), **7a** (-2.4 mV), **7b** (-3.1 mV), and **7c** (-15.3 mV), while in ascorbic acid aqueous solution (pH=4.0) were **3** (-13.3 mV), **7a** (-13.6 mV), **7b** (-14.5 mV), and **7c** (-15.8 mV). The zeta potential of the catalyst with the same dye-loading amount (5.0 μmol/g) was also measured, the values of ascorbic acid aqueous solution (pH=4.0) were **3** (-10.5 mV), **7a** (-13.6 mV), **7b** (-14.4 mV) and **7c** (-15.2 mV), which also has the same tendency as the photocatalytic hydrogen production results. With the increase of the alkyl chains, **dye**/Pt-TiO_2 became more negatively, lead the catalysts are more easily attracts ascorbic acid which has a positive potential. Therefore, the presence of ascorbic acid around the catalyst becomes more possible. The concentration of adsorbed counterion can estimate by the model of the electrical double layer.[14,34] The values of adsorbed ascorbic acid showed with saturated concentration of dye loaded photocatalyst as the order in **dye**/Pt-TiO_2 : **7c** (1.05 mol/L) > **7b** (1.00 mol/L) > **7a** (0.97 mol/L) > **3** (0.95 mol/L), while 5 μmol/g loaded **dye**/Pt-TiO_2 showed **7c** (1.05 mol/L) > **7b** (1.03 mol/L) > **7a** (0.97 mol/L) > **3** (0.86 mol/L), which suggest as the alkyl chain length was increased, the adsorbed concentration of ascorbic acid around **dye**/Pt-TiO_2 became higher. Although the zeta potential of Pt-TiO_2 alone in ascorbic acid solution (pH = 4.0) is -15.5 mV, suggesting that a similar amount of ascorbic acid as in **7c**/Pt-TiO_2 is present on the surface of Pt-TiO_2 without dye-loading, the photocatalytic hydrogen production rate at >420 nm in the presence of ascorbic acid is 101.2 $\mu mol \cdot g_{cat}^{-1} \cdot h^{-1}$. In other words, the acceleration in **dye**/Pt-TiO_2 photocatalytic activity cannot be explained solely by the difference in surface potential between ascorbic acid and titanium oxide. These surface potential differences including dye-structure dependant effect act as driving forces and lead to new secondary coordination spheres for efficient electron transfer around Pt-TiO_2.

3.8 Photocurrent and Impedance

To discuss relationship in **3** and **7a**-**7c**'s structure and the reason for the improvement of activity, photocurrent measurements were performed (Fig. 6a). As expected, all **3** and **7a**-**7c**/TiO_2 electrodes exhibit good photoelectric responsibility and cyclability, with light turned on and off. The order of photocurrent intensity is **7c** (279.3 $\mu A \cdot cm^{-2}$) > **7b** (257.9 $\mu A \cdot cm^{-2}$) > **7a** (248.3 $\mu A \cdot cm^{-2}$) ≈ **3** (242.8 $\mu A \cdot cm^{-2}$). The order of photocurrent follows the same tendency as the hydrogen production rate or TOF, as the suggested number of excited photons played a critical role in the production of hydrogen in the **dye**/Pt−TiO_2 photocatalyst system. Moreover, the photocurrent density becomes higher as the alkyl chain length was increased; thus, it can be demonstrated that the photocurrent density can be improved by increasing the number of alkyl chains. The higher photocurrent density suggested increasing of the electron carrier concentration into TiO_2 of conduction band.[35] To further discuss the effect of hydrophobicity from alkyl chain length on catalyst activity, the electrochemical impedance spectroscopy was measured at 0.0 V (vs Ag/AgCl) in dark. (Fig. 6b). All **dye**/TiO_2 electrodes consists of 3 different semicircles at high, middle, and low frequency regions.[36] R_0 represents the series resistance, R_1 and C_1 corresponds to the impedance between the current collector and the working electrode, R_2 and C_2 represents the impedance between

TiO_2, **dye** and ascorbic acid (second coordination sphere), and R_3 and C_3 represents the electron transfer at the interface between the bulk electrolyte, dye, and TiO_2. In **7c**, a minimum semicircle was observed in the intermediate frequency region, which suggests that **7c**/TiO_2 are easiest to get electron from ascorbic acid. **7c** also showcased a larger semicircle in the low frequency region indicating a higher recombination resistance (106.1 $\Omega \cdot cm^{-2}$) followed by **7b**, **7a** and **3** with 88.3 $\Omega \cdot cm^{-2}$, 77.3 $\Omega \cdot cm^{-2}$ and 74.4 $\Omega \cdot cm^{-2}$ respectively. The resistance at low frequencies represents the diffusion rate of the electrolyte in the aqueous solution, which suggests that the diffusion rate becomes slower as the alkyl chain increases. Upper results indicate that both the resistance for charge recombination and photocurrent density are increased after the increase of alkyl chains length to the dye molecules.

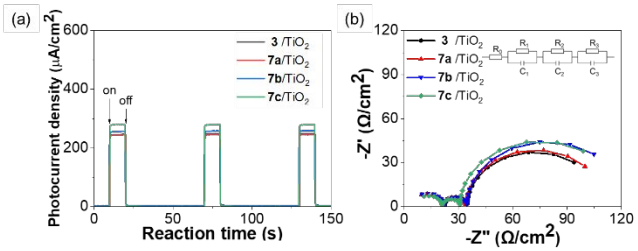

Fig. 6 (a) Photocurrent spectra of **3** and **7a**-**7c**/TiO_2. (b) Impedance spectra of **3** and **7a**-**7c** /TiO_2. (0.15 W cm^{-2}, >420 nm, 0.57 M ascorbic acid aq., 0.1 M Na_2SO_4, pH 4.0).

3.9 Time-resolved absorption measurements

To further explore the reaction mechanism, time-resolved absorption spectroscopy measurements were conducted for **3** and **7a**-**7c**/TiO_2 in 0.57 M ascorbic acid solution upon excitation at 400 nm using femtosecond pump–probe spectroscopy (Fig. 7). The spectral evolution from 0 to 200 ps is shown in Fig. S10. A negative absorption band at around <550 nm and a positive absorption band between 550 and 700 nm were observed in each dye. The negative absorption band stems from the absorption of dye at 400-550 nm due to ground state bleaching.[37] The radical cation of dye in THF solution showed at 513 nm, that means the positive peak are not belong to dye radical cation (Fig. S11). The pico-second scale generated positive absorption band between 550 and 700 nm assigned to the excited-state absorption ($S_0 \rightarrow S_1$ transition).[38,39] The data were fitted with double exponential decay function. The time decay constants τ_1, and τ_2 of dye was determined to be 84.3 ps, and 667.3 ps of **3**/TiO_2, 13.9 ps, and 356.6 ps of **7a**/TiO_2, 8.3 ps, and 144.1 ps of **7b**/TiO_2, 0.14 ps, and 29.0 ps of **7c**/TiO_2, respectively. In dye-sensitized photocatalysis system, the dye is excited to an excited state and injection into TiO_2 of conduction band or shallow trap site at 100 fs scale, then electrons are migrated to surface or deep trap sites over 100 ps. [40,41] The electrons are then transferred to a trap site or surface of the titanium dioxide where they are used for reactions. The injected electrons return to the ground state by recombining with the dye if there are not used for reaction. In the present measurement system, the ascorbic acid solution is considered to be in the vicinity of the dye, and its amount depends on the state of the second coordination sphere. Dyes with long alkyl chains, such as **7c**, have more ascorbic acid near the **dye**/TiO_2 interface, while the amount of ascorbic acid at the interface decreases for **3** and **7a-b**. If the photoexcited dye injects electrons into the TiO_2 and quickly receives electrons from the ascorbic acid, an efficient charge injection process can be formed. Both τ_1 and τ_2 of lifetime became shorter with the order of **7c** < **7b** < **7a** < **3**, suggested that dye-excited state of quenching dynamics is strongly affect with second sphere coordination environment of ascorbic acids concentration. The primary constituent (τ_1), distinguished by its short lifetime, pertains to the components of excited state dye quenching with ascorbic acid from second sphere coordination. In contrast, the second constituent (τ_2) signifies were longer in such **3**, **7a** and **7b**, suggested that the quenching of the excited state through the indirect quenching from second sphere coordination of ascorbic acid or charge recombination from injected electron on TiO_2. **3**/TiO_2 showed longest lifetime, **7c**/TiO_2 showed shortest lifetime in 4 kinds of **dye**/TiO_2. This lifetime demonstrates the speed of the dye can get electrons from ascorbic acid (AA), after electron injection into TiO_2. The excited **7c***/TiO_2 can be easier get electrons and go back to ground state, thus enter the next reaction cycle, leading to an increase in hydrogen production.

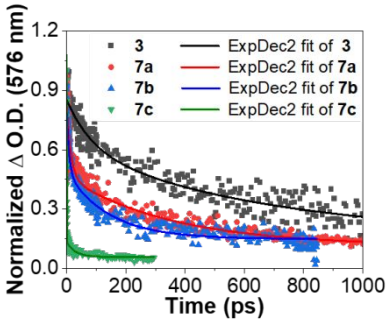

Fig. 7 Kinetic decay profiles of **3** and **7a**-**7c**/TiO_2 at 576 nm.

3.10 Proposed photocatalytic reaction mechanism

Fig. 8 shows the proposed mechanism of dye-sensitized photocatalytic hydrogen production in this work, and Fig. S12 and Table S2 shows the crucial role of hydrophobicity in the relationship between photocatalytic activity, photocurrent density, zeta potential differences with ascorbic acid, and the hydrogen production performance of the dye. Dye **3**, which possesses the weakest hydrophobicity, demonstrates the lowest photocurrent density, zeta potential differences with ascorbic acid, hydrogen production activity, and consequently, the longest decay lifetime at the excited state. In contrast, as the hydrophobicity increases, all aspects of the dye's performance improve. Notably, **7c**, with the strongest hydrophobicity, exhibits the highest photocurrent density, zeta potential differences with ascorbic acid, and the fastest charge transfer rate. These enhancements contribute to its shortest decay lifetime at the excited state, primarily attributed to its improved ability to receive electrons from ascorbic acid. Thus, the hydrophobicity of the dye plays a pivotal role in dictating its overall performance. Therefore, in this case, with the enhancement of hydrophobicity of the dye, the existence probability of ascorbic acid present is increased and the present of water molecules around the catalyst becomes less by alkyl-chain formed second sphere coordination, which leads to **7c** showing the best photocatalytic activity (Fig. 8).

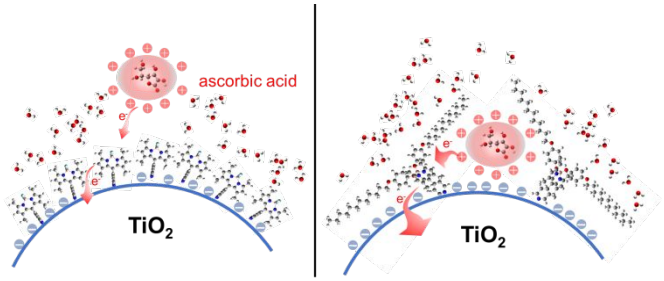

Fig. 8 Probable mechanism of photocatalytic efficient hydrogen evolution (left: **3**; right: **7c**).

4 Conclusions

To discuss the effect of −F position substituents and hydrophobicity of BODIPY dyes on photocatalytic activity, 3 dyes with different alkyl chain lengths (**7a**–**7c**) were synthesized and compared with the unsubstituted **3**. Firstly, the DFT calculations were performed to investigate the electronic structures of the dyes after substitution at the −F position. The calculations revealed that the substitution at the −F position could induce an intramolecular charge transfer (ICT) in the dyes, which results in an enhanced absorption of visible light and a higher potential for photocatalytic activity. Secondly, the effects of alkyl chain length on the photocatalytic activity of the dyes were investigated. The hydrophobic angles and impedances of the dyes increased with the increase of alkyl chain length, which resulted in a more favourable microenvironment for hydrogen production. Finally, the photocatalytic activities of the dyes were evaluated experimentally under visible light irradiation. Among the four dyes studied, dye **7c** exhibited the highest photocatalytic activity, with a hydrogen production rate of 496.5 $\mu mol \cdot g_{cat}^{-1} \cdot h^{-1}$ and an AQY at 650 nm of 1.4%. Overall, this study provides insights into the design of metal-free organic dyes with improved photocatalytic activity, also suggests that the substitution at the -F position and the optimization of the hydrophobicity could change the environment, make a new second coordination sphere to enhance the photocatalytic performance of the dyes.

Author Contributions

Synthesis of materials, X.-F., Shen and M.Watanabe; methodology, X.-F., Shen and M.Watanabe; analysis, X.-F., Shen, M.Watanabe, J. T. Song, and T., Abe; manuscript preparation, X.-F., Shen, M.Watanabe, A. Takagaki, K.Tanaka, and T.Ishihara. All authors have read and agreed to the published version of the manuscript.

Conflicts of interest

There are no conflicts to declare.

Acknowledgements

This work was supported by JST, the establishment of university fellowships towards the creation of science technology innovation, Grant Number JPMJFS2132, and by JSPS Grant-in-Aid for Scientific Research(C) Grant Number 21K04692, the Strategic International Collaborative Research Program (SICORP) concerning “Research on Hydrogen as a renewable energy carrier’’ from the Japan Science and Technology Agency (JST). M.W. and T. I. acknowledges the support from I2CNER and funded by the World Premier International Research Center Initiative (WPI), and Center for Energy Systems Design (CESD), MEXT, Japan.

References

1 N. Mariotti, M. Bonomo, L. Fagiolari, N. Barbero, C. Gerbaldi, F. Bella and C. Barolo, *Green Chem.*, 2020, **22**, 7168–7218.
2 A. Kobayashi, S. ya Takizawa and M. Hirahara, *Coord. Chem. Rev.*, 2022, **467**, 214624.
3 M. Watanabe, *Sci. Technol. Adv. Mater.*, 2017, **18**, 705–723.
4 G. Reginato, L. Zani, M. Calamante, A. Mordini and A. Dessì, *Eur. J. Inorg. Chem.*, 2020, **2020**, 899–917.
5 E. Nikoloudakis, I. López-Duarte, G. Charalambidis, K. Ladomenou, M. Ince and A. G. Coutsolelos, *Chem. Soc. Rev.*, 2022, **51**, 6965–7045.
6 S. Peiris, H. B. de Silva, K. N. Ranasinghe, S. V. Bandara and I. R. Perera, *J. Chinese Chem. Soc.*, 2021, **68**, 738–769.
7 M. Ismael, *Fuel*, 2021, **303**, 121207.
8 X.-F. Shen, M. Watanabe, A. Takagaki, J. T. Song, T. Abe, D. Kawaguchi, K. Tanaka and T. Ishihara, *Appl. Phys. A Mater. Sci. Process.*, 2023, **129**, 28.
9 Y. Zhang, J. Yang, R. Ge, J. Zhang, J. M. Cairney, Y. Li, M. Zhu, S. Li and W. Li, *Coord. Chem. Rev.*, 2022, **461**, 214493.
10 W. H. Lai, Z. Miao, Y. X. Wang, J. Z. Wang and S. L. Chou, *Adv. Energy Mater.*, 2019, **9**, 1–30.
11 A. Ghosh, S. Dasgupta, A. Kundu and S. Mandal, *Dalt. Trans.*, 2022, 10320–10337.
12 K. H. Chen, N. Wang, Z. W. Yang, S. M. Xia and L. N. He, *ChemSusChem*, 2020, **13**, 6284–6289.
13 J. Li, Y. Zhang and N. Kornienko, *New J. Chem.*, 2020, **44**, 4246–4252.
14 M. Wen, X. B. Li, J. X. Jian, X. Z. Wang, H. L. Wu, B. Chen, C. H. Tung and L. Z. Wu, *Sci. Rep.*, 2016, **6**, 29851.
15 G. Huang, Q. Yang, Q. Xu, S. H. Yu and H. L. Jiang, *Angew. Chemie - Int. Ed.*, 2016, **55**, 7379–7383.
16 L. Li, Q. Yang, S. Chen, X. Hou, B. Liu, J. Lu and H. L. Jiang, *Chem. Commun.*, 2017, **53**, 10026–10029.
17 S. Sinha, C. K. Williams and J. J. Jiang, *iScience*, 2022, **25**, 103628.
18 V. N. Nguyen, J. Ha, M. Cho, H. Li, K. M. K. Swamy and J. Yoon, *Coord. Chem. Rev.*, 2021, **439**, 213936.
19 D. Chen, Z. Zhong, Q. Ma, J. Shao, W. Huang, X. Dong and X. Dong, *ACS Appl. Mater. Interfaces*, 2020, **12**, 26914–26925.
20 X.-F. Shen, M. Watanabe, A. Takagaki, J. T. Song and T. Ishihara, *Catalysts*, 2020, **10**, 535.
21 N. A. Bumagina, E. V. Antina, A. A. Ksenofontov, L. A. Antina, A. A. Kalyagin and M. B. Berezin, *Coord. Chem. Rev.*, 2022, **469**, 214684.

22 D. Ho, R. Ozdemir, H. Kim, T. Earmme, H. Usta and C. Kim, *ChemPlusChem*, 2019, **84**, 18–37.
23 M. Wang, S. Su, X. Zhong, D. Kong, B. Li, Y. Song, C. Jia and Y. Chen, *Nanomaterials*, 2022, **12**, 1918.
24 E. Bodio and C. Goze, *Dye. Pigment.*, 2019, **160**, 700–710.
25 J. A. Jacob-Dolan, M. D. Capobianco, H. Y. Liu, C. Decavoli, R. H. Crabtree and G. W. Brudvig, *Dalt. Trans.*, 2022, **51**, 14260–14266.
26 N. Umeda, H. Takahashi, M. Kamiya, T. Ueno, T. Komatsu, T. Terai, K. Hanaoka, T. Nagano and Y. Urano, *ACS Chem. Biol.*, 2014, **9**, 2242–2246.
27 N. M. O'Boyle, A. L. Tenderholt and K. M. J. Comp. Chem., 2008, **29**, 839-845.
28 M. Hecht and F. Würthner, *Acc. Chem. Res.*, 2021, **54**, 642–653.
29 J. Xu, L. Wen, W. Zhou, J. Lv, Y. Guo, M. Zhu, H. Liu, Y. Li and L. Jiang, *J. Phys. Chem. C*, 2009, **113**, 5924–5932.
30 J. Warnan, J. Willkomm, J. N. Ng, R. Godin, S. Prantl, J. R. Durrant and E. Reisner, *Chem. Sci.*, 2017, **8**, 3070–3079.
31 D. Rajaraman, G. Sundararajan, R. Rajkumar, S. Bharanidharan and K. Krishnasamy, *J. Mol. Struct.*, 2016, **1108**, 698–707.
32 X. Zhang, T. Peng and S. Song, *J. Mater. Chem. A*, 2016, **4**, 2365–2402.
33 R. Figueroa-Méndez and S. Rivas-Arancibia, *Front. Physiol.*, 2015, **6**, 1–11.
34 T. W. Heady, T. W. Healy, D. W. Fuerstenau and D. Waals, *J. Phys. Chem.,* 1964, **497**, 3562–3566.
35 W. Yang, R. R. Prabhakar, J. Tan, S. D. Tilley and J. Moon, *Chem. Soc. Rev.*, 2019, **48**, 4979–5015.
36 A. Sacco, *Renew. Sustain. Energy Rev.*, 2017, **79**, 814–829.
37 S. Y. Kim, Y. J. Cho, H. J. Son, D. W. Cho and S. O. Kang, *J. Phys. Chem. A*, 2018, **122**, 3391–3397.
38 T. Suhina, S. Amirjalayer, S. Woutersen, D. Bonn and A. M. Brouwer, *Phys. Chem. Chem. Phys.*, 2017, **19**, 19998–20007.
39 Y. Zhou, W. Ni, L. Ma, L. Sun, J. Zhao and G. G. Gurzadyan, *J. Phys. Chem. C*, 2022, **126**, 17212–17222.
40 N. J. Cherepy, G. P. Smestard, M. Grätzel, and J. Z. Zhang, *J. Phys. Chem. B,* 1997, **101,** 9432-9351
41 S. Kaniyankandy, S. Verma, J. A. Mondal, D. K. Palit and H. N. Ghosh, *J. Phys. Chem. C,* 2009, **113,** 3593-3599.